A Validity Study for Perfusion in the Capillary System

Constantin Heck, Erik A. Hanson,
Arvid Lundervold, Jan Modersitzki, Alexandre Malyshev, Erlend Hodneland
(random order)

Thursday 7th May, 2015

Contents

1 Introduction

Quantitative medical measurements based on tracer kinetic models has for many years been an important field both in research and in clinical practice [1, 2, 3]. In the present work we will focus on mathematical methods for estimation of blood perfusion in the brain (cerebral blood flow) based on dynamic MR imaging. Still, the theory covered here, will also be of relevance in general perfusion studies.

While limitations in medical imaging for decades have confined studies to only handle larger tissue regions or full organs, modern MR technology and voxel based analysis give rise to aspirations about detailed perfusion maps with millimeter precision. Examples of successful estimations of parameter maps are found in i.e. [?]. The perfusion maps (and other parameter maps) combines the quantitative nature of the tracer kinetic model with important qualitative anatomical information. The maps have proven to be of particular value in e.g. stroke studies [?]. Among the physiological parameters obtainable from tracer kinetic models, the perfusion (or CBF) has proven to be particularly difficult to reliably describe on a voxel-basis [4]. In several studies, perfusion or CBF are therefore only reported in relative values and the corresponding parameter maps are only used in a qualitative manner [5]. The methodological limitations in perfusion estimation are caused both by issues in the numerical implementation, but also by the basic formulation of the model itself. It is has been widely studied how delay and dispersion of the contrast bolus between the AIF and the voxel as well as assumptions about directional flow [6, 7] effects the perfusion estimation. In [7] mathematical theory for flow field models are introduced and proposed as an alternative to the classical models for perfusion on voxel level. In this work we will use some of the same physical concepts, but also relate them to the classical perfusion models. We will further discuss limitations of classical voxel based perfusion models and focus on their validity in an unstructured flow field. The models, and how they behave under different ROI/voxel sizes and shapes, are analyzed mathematically and evaluated in a synthetic flow field. We will also derive a mathematical framework in which the medical notion of perfusion can be understood in a physical precise manner.

An evaluation of perfusion models using a synthetic flow field is also performed in i.e. [8]. Here, the synthetic model is based on solution of Navier-Stokes equations within the arterial system and the effect of dispersion is studied. In the present work, we model the contrast agent (CA) propagation through a small section of the capillary system. Both these approaches require several clarifying assumptions on flux and propagation. In pharmacokinetic analysis it is often assumed that each ROI (voxel) is an autonomous system that can be modeled by standard pharmacokinetic theory [?]. As in [8], we study CA propagation through a larger area with a highly developed capillary/arterial system and thereby consider a range of connected problems where each voxel can be regarded as an inlet for the surrounding voxels. Further, the CA propagation is modeled as a spatially coupled transport process, which more accurately mimics the nature of the blood flow in the tissue. Unlike Calamante et al. we also distinguish between the (scalar) perfusion

maps, describing flow normalized over a volume, and the physical (vector valued) flow field, describing flow normalized over a surface area.

The rest of this paper is arranged as follows: In Section 2, we outline a classical method for perfusion estimation and discuss two solution methods within the framework of deconvolution. In Section 3 we describe how a synthetic flow field in the capillary system can be modeled using simple models from porous media literature. We also discuss the mathematical resembling between the flow field models and the classical theory outlined in Section 2. In Section 7 evaluate the performance of the classical models by applying them on synthetic flow fields. The results and concluding remarks are summarized in section 8.

2 Classical Models

We will first describe two standard models to recover CBF,CBV and MTT from data displaying propagation of a contrast agent through the tissue. The so-called Deconvolution Model (DM) is used in vast amount of publications [9, 10, 11, 12, 13]. Restoration of CBF yields reasonable results [?], however validation is still a problem as ground-truth CBF is hard to determine. Validation of novel implementations is usually done in the so-called *inverse crime* setting. This means that the forward model to generate data and the backward model to reconstruct parameters are similar, if not identical. Another model which has been shown to exhibit good properties in restoring CBF and MTT is the so-called Maximum Slope Model (MS) [14, 15]. The maximum slope model has been shown to exhibit advantages over the deconvolution model especially if uptake curves are degraded in the late phase [10]. However, since it relies on point-wise estimates, application to real data is nevertheless difficult and prone to noisy measurements. Also, the maximum slope model inherently assumes that no outflow takes place when the AIF peaks (see Sec. 2.3). This assumption is questionable for arbitrary, maybe pathological tissue [?].

Following [13], we now briefly present the theoretical basis of two models. Let Ω_i be a control volume with one inlet and one outlet and let $C(t)$ denote the CA concentration within Ω_i at timepoint t. Let us furthermore assume linearity and stationarity of CA in- and outflux with proportionality constants $P_\mathrm{a}, P_\mathrm{v}$, given in $\mathrm{mm}^3/(\mathrm{s}\,\mathrm{mm}^3)$. These assumptions lead to the differential equation $C'(t) = P_\mathrm{a} c_\mathrm{a}(t) - P_\mathrm{v} c_\mathrm{v}(t)$. Here $c_\mathrm{a}, c_\mathrm{v}$ are the CA concentrations at the inlet and outlet of Ω_i. Assuming incompressibility of flow leads to $P_\mathrm{a} = P_\mathrm{v}$ and hence we obtain the general form

$$C'(t) = P_\mathrm{a} \left(c_\mathrm{a}(t) - c_\mathrm{v}(t) \right). \tag{1}$$

In the next step, the deconvolution model and the maximum slope model are making different assumptions.

2.1 The Convolution Model: Theory and Implementation

For the deconvolution model it is assumed that there is a probability distribution of transit times $h(t)$ through Ω_i. This leads to

$$c_{\mathrm{v}}(t) = (h * c_{\mathrm{a}})(t) := \int_0^t c_{\mathrm{a}}(s)h(t-s)\,\mathrm{d}s.$$

Combining this with (1) yields $C'(t) = P_{\mathrm{a}}c_{\mathrm{a}}(t) - P_{\mathrm{a}}(h * c_{\mathrm{a}})(t)$. Integrating this equation and using basic properties of the convolution one obtains

$$C(t) = (I * c_{\mathrm{a}})(t). \tag{2}$$

Here the *impuls-response function* I is defined as $I(t) := P_{\mathrm{a}}(1 - \int_0^t h(s)\,\mathrm{d}s)$. One can show that I fulfills the following properties:

- $I(0) = P_{\mathrm{a}}$,
- I is monotonously decreasing,
- $I \geq 0$.

The problem to identify I given a tissue curve C and an arterial input function c_{a} is a deconvolution problem. If I is recovered, P_{a} can subsequently be estimated as $P_{\mathrm{a}} = \max_t I(t)$. There are several methods to perform the deconvolution. A standard approach using Fourier-based algorithms has been shown sensitivity in the presence of noise [16, 9]. Another class of deconvolution algorithms gaining increasing attention are based on Bayesian modeling [17, 18]. Recent evaluations are showing good performance [19], however the numerical handling is still difficult since complex numerical integrations have to be performed. The class most popular among deconvolution algorithms is based on singular value decomposition (SVD) [9]. These algorithms have been shown to be quite robust in the presence of noise. Also, they can be easily adapted to be robust against delays in tracer arrival using block-circular structures (bSVD cf. [20]). In order to identify the impuls-response functions I from the simulated data, we hence decided to use the bSVD model as proposed in [20].

2.2 The Convolution Model for a Well-Mixed Compartment

If we assume that Ω_i is a well-mixed compartment where $C(t) = \phi c_{\mathrm{v}}(t)$ for some $0 \leq \phi \leq 1$, equation (1) reduces to the initial value problem

$$\begin{aligned}(\phi c_{\mathrm{v}})' &= P_{\mathrm{a}}c_{\mathrm{a}} - P_{\mathrm{a}}c_{\mathrm{v}},\\ c_{\mathrm{v}}(0) &= 0.\end{aligned}$$

Letting $\mathrm{MTT} := P_{\mathrm{a}}/\mathrm{CBV}$ yields the solution

$$C(t) = P_{\mathrm{a}} \int_0^t e^{-1/\mathrm{MTT}(t-s)} c_{\mathrm{a}}(s)\,\mathrm{d}s$$

with residue function $R(t) = e^{-t/\mathrm{MTT}}$.

2.3 The Maximum Slope Model: Theory and Implementation

In the MS Model it is assumed that at the beginning no or only a negligible amount of CA is leaving the system (cf. [15]). For this time (1) reduces to

$$C'(t) = P_{\mathrm{a}} c_{\mathrm{a}}(t).$$

It is furthermore assumed this assumption is valid for the timepoint where c_{a} peaks. In this case one can see that if c_{a} has a maximum also C' must have a maximum. Hence it holds that

$$P_{\mathrm{a}} = \frac{\max_t C'(t)}{\max_t c_{\mathrm{a}}(t)}. \tag{3}$$

3 The Novel Synthetic Model

Structurally, the model-assumptions for both classical methods presented in Section 2 are similar. Both are assuming that the region of interest where the model is applied exhibits only one inlet and one outlet. In fact, this assumption is questionable when we describe CA propagation through a larger area with a highly developed capillary system. Here we expect in contrast a coupled systems, since each voxel can be regarded as an inlet for the surrounding voxels. We hence decided to describe the CA propagation as a spatially coupled transport process. Details of the modeling of transport will be presented in Section 3.2.

Since the CA transport itself is driven mainly by blood flow, we will describe a simple model for the blood flow through capillary tissue in Section 3.1. Within the capillary system we expect the blood flow to be driven mainly by differences in pressure. This way of modeling flow comes from the theory of porous media and is expressed in Darcy's law [?]. As a consequence, we will also apply the physical understanding of flow as vector valued surface flux $q = q(x)$ with units $\mathrm{mm}^3/(\mathrm{s}\,\mathrm{mm}^2)$. The surface flux is a vector field describing the volume of fluid per unit time flowing across a sliced unit area of the sample. A model to convert vector valued flux to scalar perfusion with units $\mathrm{mm}^3/(\mathrm{s}\,\mathrm{mm}^3)$ will be introduced in Section 4.1. In our modeling, CA flux $J(x,t)$ with units $\mathrm{mmol}/(\mathrm{s}\,\mathrm{mm}^2)$ is assumed to be linear and stationary, meaning that $J(x,t) = q(x) \cdot c(x,t)$. Apart from the normalization with respect to surface, the assumptions of linearity and stationarity are in complete agreement with standard pharmacokinetic modeling [13]. A detailed description of modeling the blood flow can be found in Section 3.1.

Another key ingredient from porous media is the introduction of the porosity ϕ for $0 \leq \phi \leq 1$. The porosity describes which fraction of a small tissue volume is accessible for blood. Comparing with pharmacokinetic modeling, the porosity directly translates to the cerebral blood volume (CBV).

We will now describe the construction of the digital phantom in detail.

3.1 Modeling the Blood Flow

We model the blood flow as the flow of a fluid through a porous medium. The fluid has units $\mathrm{mg/mm^3}$ and is denoted by $\rho = \rho(x,t)$. As explained previously, the flux q (in $\mathrm{mm^3/(s\,mm^2)}$) as well as the porosity ϕ (with $0 \leq \phi \leq 1$) are assumed to be stationary and hence independent of time. Fluid introduced and extracted from the system is modeled by a source- and sink term $\tilde{Q} = \tilde{Q}(x)$ with units $\mathrm{mg/(s\,mm^3)}$. The continuity equation describing conservation of mass now states that

$$\frac{\partial(\phi\rho)}{\partial t} + \nabla \cdot (\rho q) = \tilde{Q}. \tag{4}$$

Furthermore assuming that the system is in steady-state and that the density of blood $\rho(x)$ is constant in space, we obtain that $\frac{\partial \rho}{\partial t} = 0$ and hence:

$$\nabla \cdot q = \frac{\tilde{Q}}{\rho}. \tag{5}$$

In order to scale away the density ρ we define another source term Q with units $\mathrm{mg/(s\,mm^3)}$ having the relation $Q := \tilde{Q}\rho$, thus transforming (5) into

$$\nabla \cdot q = Q. \tag{6}$$

The right hand side is only non-zero within the source or the sink. Elsewhere, (6) is concurrent with the incompressibility condition of divergence free flow.

Low velocity fluid flux in porous media is described by Darcy's law [?]:

$$q = -\frac{K}{\mu}\left(\nabla p + \rho g \nabla z\right).$$

here g is the gravitational acceleration, K is the permeability tensor with units $\mathrm{m^2}$, z is the spatial position along the gravitational field and $\mu = \mu(x)$ is the viscosity of the fluid with units Pa s. For the current project the flux is taking place perpendicular to the gravitational field and the gravitational term can thereby be discarded. That a simplified version of Darcy's law thus becomes

$$q = -\frac{K}{\mu}\nabla p. \tag{7}$$

We now combine (6) and (7) and assume that K is symmetric and positive definite. This yields the following elliptic partial differential equation the pressure-field p with units Pa must fulfill:

$$\left| \begin{array}{ll} \nabla \cdot \left(-\frac{K}{\mu}\nabla p\right) = Q & x \in \Omega, \\ n \cdot \nabla p = 0 & x \in \partial\Omega. \end{array} \right| \tag{8}$$

Here $\partial\Omega$ denotes the boundary of Ω and n the outward unit normal vector. Modeling an isolated system with no inflow or outflow along the boundary of Ω, we impose the

Neumann boundary conditions $n \cdot \nabla p = 0$ on $\partial\Omega$. Note that (8) exhibits a solution which unique up to constant since only pressure differences are taken into consideration [21]. Having solved (8) the flux field can be computed according to (7) from the obtained pressure map.

3.2 Modeling the Contrast Agent Transport

In this section we will describe how the CA propagates in the tissue according to the flow-field. We assume that the CA is introduced at a source- and extracted at a sink location. The concentration map resulting from the simulation is later used to model the CA concentration one would observe with MRI or CT measurements.

In order to define meaningful continuous contrast agent concentrations, we first describe the CA concentration in an (arbitrarily) small tissue volume Ω_i. Assume that V_i is the volume of Ω_i and v_i the the blood volume of Ω_i. By definition the porosity is in this case given by $\phi_i = v_i/V_i$. Let $C_i(t)$ denote the CA concentration in Ω_i with respect to the whole volume V_i at timepoint t. The CA concentration with respect to the blood volume v_i will be denoted by $c_i(t)$. Both concentrations have units mmol/mm^3. From the definition of c_i, C_i and ϕ_i we obtain the relation $C_i(t) = \phi_i \cdot c_i(t)$.

The rate of change of tracer molecules within the control volume Ω_i can he described by

$$\frac{\mathrm{d}}{\mathrm{d}t} \int_{\Omega_i} C_i(t)\,\mathrm{d}x = \int_{\Omega_i} \frac{\mathrm{d}}{\mathrm{d}t}(\phi_i c_i(t))\,\mathrm{d}x. \tag{9}$$

Since we expect mainly transport along the vessels and marginal diffusion, the change in tracer mass within Ω_i occurs only from advective flow and the source and sink field Q. Let us write the source- and the sink term as $Q = Q_{\mathrm{si}} + Q_{\mathrm{so}}$ where $Q_{\mathrm{si}} \leq 0$ is the sink and $Q_{\mathrm{so}} \geq 0$ is the source. Both are assumed to be zero everywhere except at in the respective source and sink locations. Note that $Q = Q_{\mathrm{so}} + Q_{\mathrm{si}}$ and $\int_\Omega Q\,\mathrm{d}x = 0$ in line with incompressible flow. The change in contrast agent at time point t can hence be written as

$$-\int_{\Gamma_i} c_i(t)(q_i \cdot n)\,\mathrm{d}s + \int_{\Omega_i} c_{\mathrm{a}}(t) Q_{\mathrm{so}}\,\mathrm{d}x + \int_{\Omega_i} c_i(t) Q_{\mathrm{si}}\,\mathrm{d}x, \tag{10}$$

where n is the outward unit normal on $\Gamma_i := \partial\Omega_i$. Furthermore $c_{\mathrm{a}}(t)$ with unit mmol/mm^3 describes the amount of contrast agent entering the system at the source. In standard pharmacokinetic modeling, c_{a} is referred to as the arterial input function (AIF). From preservation of the tracer mass, equations (9) and (10) must balance such that

$$\int_{\Omega_i} \frac{\mathrm{d}}{\mathrm{d}t}(\phi_i c_i(t))\,\mathrm{d}x + \int_{\Gamma_i} c_i(t)(q_i \cdot n)\,\mathrm{d}s = \int_{\Omega_i} c_{\mathrm{a}}(t) Q_{\mathrm{so}}\,\mathrm{d}x + \int_{\Omega_i} c_i(t) Q_{\mathrm{si}}\,\mathrm{d}x. \tag{11}$$

Upon application of the divergence theorem, (11) is consistent with the continuity equation on local form

$$\left| \begin{array}{ll} \phi \dfrac{\partial c}{\partial t} + \nabla \cdot (cq) = c_{\mathrm{a}} Q_{\mathrm{so}} + c Q_{\mathrm{si}} & x \in \Omega,\ t > 0, \\ c = 0 & x \in \Omega,\ t = 0. \end{array} \right| \tag{12}$$

This is a linear transport equation in $c(x,t)$. Assuming that ϕ is Lipschitz continuous and that $Q_{\mathrm{so}}, Q_{\mathrm{si}}, c_{\mathrm{a}}$ are continuous, we can follow that q is as the solution of (8) also Lipschitz continuous. In this case we can follow [21] to see that (12) exhibits a unique local solution.

4 Relating the Classical and the Synthetic Model

Here is still some motivation missing.

In order to test the standard models for their abilities to restore CBF and CBV, we need to convert the flux q with units $\mathrm{mm}^3/(\mathrm{s}\,\mathrm{mm}^2)$ to perfusion P with units $\mathrm{mm}^3/(\mathrm{s}\,\mathrm{mm}^3)$. A method to do that will be presented in Section 4.1. In Section 4.2 we will give a proof that the porosity CBV can be estimated from the standard relationship $\mathrm{CBV} = \left(\int_0^\infty C(x,s)\,\mathrm{d}s\right) / \left(\int_0^\infty c_{\mathrm{a}}(s)\,\mathrm{d}s\right)$.

4.1 Converting Flow to Perfusion

The model described in (8) uniquely determines the flux field $q(x)$. However, in pharmacokinetic modeling the parameter of interest is usually the cerebral blood flow (CBF), which we will denote by $P(x)$. It is not obvious how to transform a flux field into a scalar perfusion field $P(x)$. There are at least two obvious differences between q and P. First, the flux is a vector field and the perfusion is a scalar field. Second, the flux relates to a surface area and the perfusion relates to a volume. Thus, these to quantities are strictly, mathematically different but still conceptually related. In the following we describe a method for converting flux into perfusion.

The classical understanding of perfusion is the amount of blood feeding a tissue volume per unit time. Thus, the perfusion P has the units $\mathrm{mm}^3/(\mathrm{s}\,\mathrm{mm}^3)$. It is common to scale this quantity to normalized perfusion $P_n(x)$ with units ml/min/100ml. One approach for converting flux into perfusion could be to estimate the perfusion as the total inflow (or outflow) of fluid (e.g. arterial blood) into a control region per unit time, and then normalizing with the control region volume. This is only a valid approach if every control region is separated from other control regions, and not feeding each other. Thus, this approach is valid for an entire organ being the control region. Such understanding is in line with the understanding of classical compartment models for perfusion where each voxel has its own source of feeding arterial blood, independent of the neighbor voxels. Clearly, this is a simplification since voxels will be fed by their neighbors. In our synthetic

flow model SFM as well as in normal tissue this assumption is violated since the voxels are feeding their neighbor voxels with arterial blood. Simply summing the total inflow into a voxel and dividing by the voxel volume will strongly over-estimate the perfusion since we would divide by the wrong normalization volume. The problematic issue is that the incoming blood is feeding more voxels than the current voxel. This phenomenon is demonstrated in Fig. 1 where the volume on the left has the true perfusion value of $P_1 = F_0/(2V)$ for an incoming flow F_0 in mm^3/s and distribution volume $2V$ in l. However, for another discretization as shown in the middle, the perfusion within each of these sub-volumes becomes $P_2 = F_0/V = 2P_1$. Taking the average across both sub-volumes, it is clear that the perfusion is over-estimated with a factor of two. A discretization dependent perfusion value is not desirable, and the perfusion estimate of P_2 is clearly wrong.

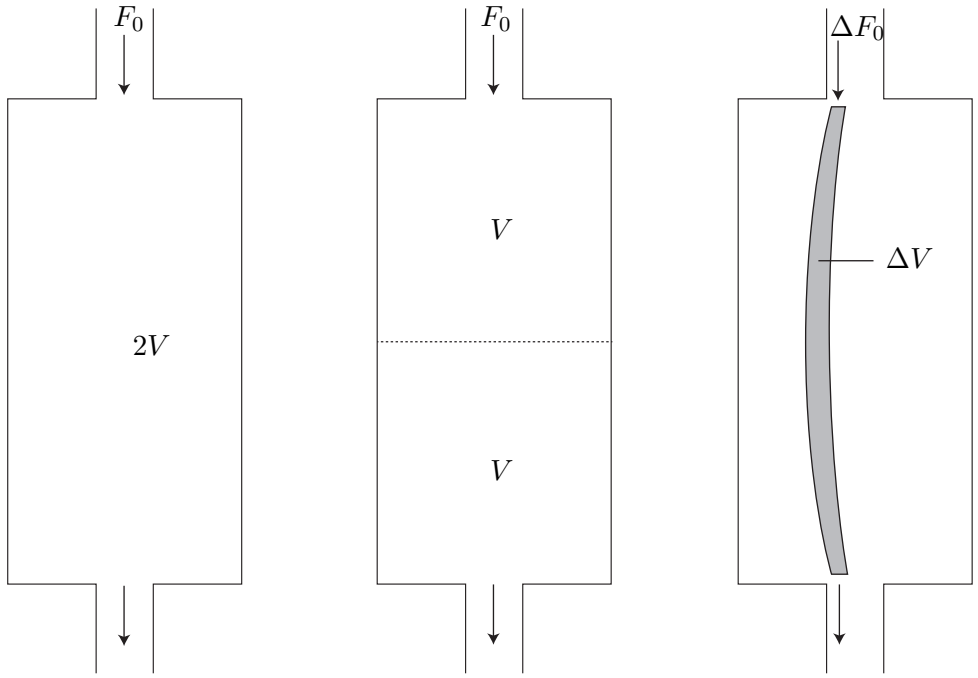

Figure 1: Perfusion within a small volume. Left: A compartment with volume $2V$ is exposed to a flow F_0 mm^3/s of fluid. From definition, the overall perfusion within this object becomes $P_1 = F_0/(2V)$ mm^3/(s mm^2). Right: The volume is divided into two smaller compartment (e.g. voxels), and the perfusion for each of the compartments becomes $P_2 = F_0/V = 2P_1$. This discrepancy between the two discretisation regimes occurs because the flow is counted twice as it is fed from one voxel to the other. Right: As a solution to the described problem we pick out a true distribution volume ΔV (area in this 2D sketch), which is a small area around a given streamline along the centre line of the grey area. This is the true distribution volume (area) which is feeded with arterial blood from the incoming fractional flow ΔF_0. The correct perfusion within ΔV is therefore $\Delta F_0/dV$. The entire compartment can further be divided into infinitesimal distribution volumes, thus providing voxelwise perfusion values.

The reason for this discrepancy is that for P_2 the perfusion has been counted twice since we are dividing by the wrong distribution volume. Instead, we need to consider to the classical definition of perfusion. The concept of perfusion has a very precise meaning, as the amount of arterial blood per time unit delivered to a capillary bed in a biological tissue, and then scaled by the feeded tissue volume. Therefore, we must divide the incoming flow by the total distribution volume that is covered by the fluid streamlines. This formulation coincides with the classical understanding of perfusion, and the correct distribution volume will rather be the volume that the fluid particles within an infinitesimal cross-sectional area around the streamlines are covering. Assuming laminar flow, the streamlines are not crossing each other and we can estimate the true distribution volume

that is fed by a given arterial blood flow.

Let us fix a point $y \in \Omega$. Formally, the direction of the streamline passing y is identical to the flux $q(y)$ at this location. Let A_ε be a 2-D disc with radius ε which is orthogonal to $q(y)$. The total volume flow mm^3/s over the disc can be expressed as

$$F = \int_{A_\varepsilon} (q \cdot n) \, \mathrm{d}A = \int_{A_\varepsilon} \left(q \cdot \frac{q(y)}{\|q(y)\|} \right) \mathrm{d}A.$$

Consider now a (unique) streamline passing through y of length L as well as a small tube of radius ε around the streamline. Following Cavalieri's principle the volume V of the tube can be expressed as $V = \varepsilon^2 \pi L$ Hence we can express the perfusion P_ε for this volume as

$$P_\varepsilon = \frac{F}{V} = \frac{1}{\varepsilon^2 \pi L} \int_{A_\varepsilon} \left(q \cdot \frac{q(y)}{\|q(y)\|} \right) \mathrm{d}A.$$

Letting $\varepsilon \to 0$ and using that $F/(\varepsilon^2 \pi)$ goes to $\|q(y)\|$ if $q(x)$ is continuous yields a locally defined value for the perfusion P_y:

$$P_y = \frac{\|q(y)\|}{L} \tag{13}$$

where L is the length of the streamline passing through the point y. This is an explicit formula for converting flux into perfusion and is later used for evaluation of the classical model for perfusion.

4.2 A Method to Estimate the Porosity

The principle of mass balance of fluid and tracer particles is described by (8) and (12). For locations x where $Q(x) = 0$ one can see that (12) becomes

$$\phi \frac{\partial c}{\partial t} = -q \cdot \nabla c.$$

Integrating from t_0 to t_1 results in the model

$$\phi[c(x, t_1) - c(x, t_0)] = -\int_{t_0}^{t_1} q \cdot \nabla c \, \mathrm{d}t.$$

Going to the limit $t_0 = 0$ to $t_1 = \infty$, using the boundary conditions $c(x, 0) = c(x, \infty) = 0$ and defining $E(x) := \int_0^\infty c(x, s) \, \mathrm{d}s$ leads to

$$0 = q \cdot \nabla E(x).$$

We can interpret this equation in such a way, that q lies in-plane with the level-sets of the function $E(x)$. This means that $E(x)$ is constant along the streamlines of the fluid

flow. Since we assumed that Q has a delta-like structure and since all streamlines are emerging at the arterial-input, we obtain

$$\int_0^\infty c(x,s)\,\mathrm{d}s = \int_0^\infty c_\mathrm{a}(s)\,\mathrm{d}s.$$

Using $C(x,t) = \phi(x)c(x,t)$ we obtain

$$\phi(x) = \frac{\int_0^\infty C(x,s)\,\mathrm{d}s}{\int_0^\infty c_\mathrm{a}(s)\,\mathrm{d}s}. \tag{14}$$

This expression coincides with the classical formula for CBV and is hereby proven analytically for the proposed model.

5 Numerical Implementations

In this section we will describe how the model was implemented numerically. For simplicity we will assume that the domain is discretized by a regular cartesian grid of size $n \times n$ with a regular cell-spacing h. The proposed method may be extended for non-regular grids in an analogous fashion.

Since conservation of mass is a key factor for both the discretization of the flow and the transport, we use algorithms preserve mass also in the simulations. To solve (8) we used the two-point flux approximation finite volume method (TPFA) [?]. Based on mass balance equations, we calculated the flux in such a fashion that conservation of mass was guaranteed. The transport equation (12) was solved by applying a straight-forward upwind scheme to (11) [?].

5.1 Discretization of the Single Phase Flow Model using TPFA

We now shortly describe the direct application of the two-point flux approximation method [?]. Considering (8) on a small domain (voxel) $\Omega_i \subset \Omega$ and applying the divergence theorem yields:

$$\int_{\partial\Omega_i} -(\lambda\nabla p)\cdot\nu\,\mathrm{d}s = \int_{\Omega_i} Q\,\mathrm{d}x \tag{15}$$

with conductivities $\lambda := K/\mu$. Defining $\Gamma_{i,j}$ as the boundary between neighboring voxels Ω_i and Ω_j, one can see that mainly the component perpendicular to Γ_{ij} will drive the flow between these voxels. The component of ∇p pointing along the normal vector of Γ_{ij} can therefore be replaced in terms of the cell centered pressure values p_i and p_j

$\Delta_h p_{ij} := \frac{(p_j - p_i)}{h}$, where h denotes the grid-spacing. The total flux across the face Γ_{ij} can hence be approximated by

$$\Delta_h p_{ij} \int_{\Gamma_{ij}} \lambda \, \mathrm{d}s \approx (p_i - p_j) \underbrace{\frac{\lambda_{ij} |\Gamma_{ij}|}{h}}_{:= t_{ij}}.$$

Here $|\Gamma_{ij}|$ is notation for the surface area of Γ_{ij} and λ_{ij} denotes an approximation of the mean conductivity on Γ_{ij}. The terms not depending on the pressure p are collected into the transmissibilities $t_{ij} := |\Gamma_{ij}| \lambda_{ij} / h$. Defining furthermore $F_i := \int_{\Omega_i} Q \, \mathrm{d}x$ yields an approximation of (15), a linear system which can be solved for the pressure p by a suitable solver. Note that p, K and μ are assumed to be given cell-centered whereas the resulting flux is discretized on a staggered grid, corresponding to the voxel faces.

5.2 Discretization of the Transport Equation

The transport described in (11) was numerically implemented using an upwind Godunov scheme [?]. Let c_i be a cell centered voxel tracer concentration and let Γ_{ij} be the face between voxel i and j with outer unit normal n_{ij}. Let q be the flux-field. Then the total CA-flow over the face Γ_{ij} can be estimated by

$$\int_{\Gamma_{ij}} (c_i q) \cdot n_{ij} \, \mathrm{d}s \approx c_i q_{ij} |\Gamma_{ij}|.$$

Keeping track of in- and outflow for each voxel and applying a straight-forward discretization of (11) yields an explicit discretization scheme to set up the transport simulation. A conversion of c_i into C_i is performed via the relation $C_i = c_i \phi_i$. The overall concentration map C_i is later used for the inverse problem of restoring CBV and CBF.

6 Experiments

We will now describe the numerical experiments we performed. Based on (8) and (12) we set up a forward simulation of blood-flow through the capillary system. A table of parameter values used for the numeral simulations are shown in Table 1. We aimed at creating a transparent synthetic test case and kept all optional parameters as simple as possible. Therefore, the permeability and porosity were assumed constant in space and in time. The voxel-wise perfusion field P was calculated according to (13). The source term was chosen to the upper left voxel and the sink term was chosen in the lower right voxel. To model the arterial-input function, we chose a standard model [9] given by the gamma-variate [22] function

$$c_\mathrm{a}(t) := (t - t_0)^\alpha e^{-(t - t_0)/\beta}$$

for $\alpha = 3$, $\beta = 1.5\,\mathrm{s}$ and $t_0 = 0\,\mathrm{s}$.

Table 1: Parameters used in the numerical experiments, optimized for a slab of the capillary system in the human brain. In order to keep all parameters as simple as possible, permeability was assumed to be isotropic and permeability, porosity and viscosity were assumed constant.

Description	Symbol	Value(s)	Unit
Concentration w.r.t. fluid space	c	-	$\mathrm{mmol/mm^3}$
Concentration w.r.t. ROI	C	-	$\mathrm{mmol/mm^3}$
CA Flux	J	-	$\mathrm{mmol/(s\,mm^2)}$
Average input perfusion	$\overline{P}$	50	ml/min/100ml
Flow source, derived from $\overline{P}$	F_{so}	0.83	$\mathrm{mm^3/s}$
Flow sink	F_{si}	$-F_{so}$	$\mathrm{mm^3/s}$
Dynamic viscosity blood [23]	μ_b	5×10^{-6}	kPa s
Fluid density blood [24]	ρ	1	$\mathrm{mg/mm^3}$
Permeability	k	5×10^{-6}	$\mathrm{mm^2}$
Porosity[20]	ϕ	0.05	$\mathrm{mm^3/mm^3}$
Spatial resolution	-	$(64, 64, 1)$	-
Physical dimension	-	$(10, 10, 1)$	mm
Voxel size	-	$(0.156, 0.156, 1)$	mm

In order to compare the Porous Media Model to the standard convolution model described in Section 2.1, an additional convolution dataset was built. The convolution dataset (convM) was set up assuming voxel-wise well-mixed compartments described in Section 2.2 and the perfusion values described in (13). Note that this assumption is in contradiction to the assumptions of the maximum-slope model. We can hence not expect to recover reasonable perfusion parameters from convM using the maximum slope model. A comparison of the tissue curves at different positions of the tissue can be found in Figure 3.

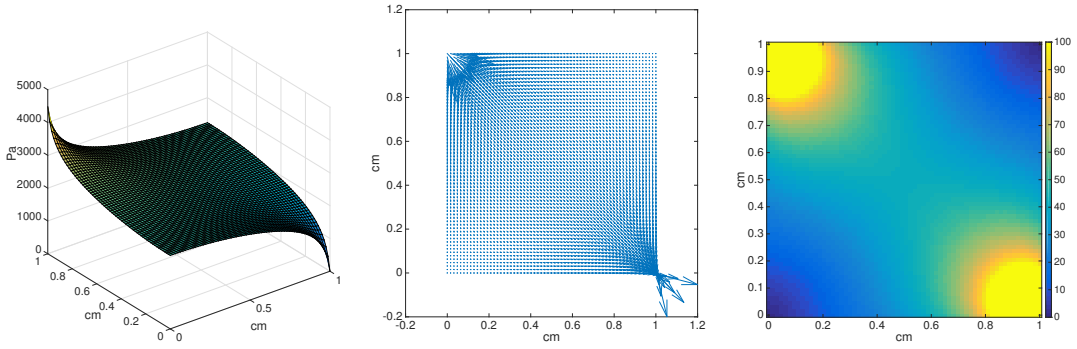

(a) Pressure field p (b) Flow field q (c) Perfusion P.

Figure 2: Synthetic flow model with a source in the upper left corner and a sink in the lower right corner. (a) Pressure field from solving the linear system in (8), in Pa (b) flux field, (c) Voxelwise perfusion according to (13) in $\mathrm{mm^3/(s\,mm^3)}$.

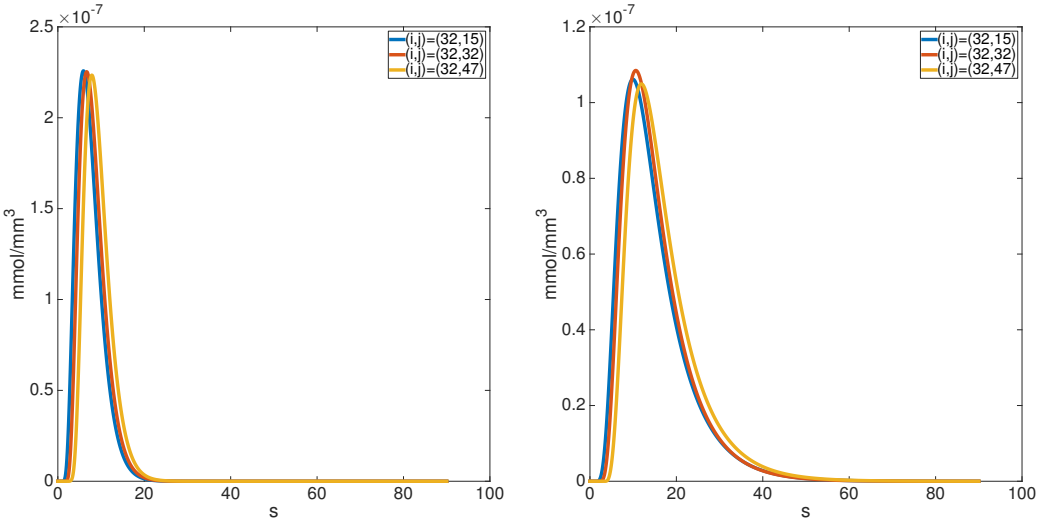

(a) Porous Media Model (b) Convolution Model

Figure 3: Comparison of tissue curves in the Porous Media (a) and the Convolution Model (b). Curves were sampled in the middle row $i = 32$ and columns $j \in \{15, 32, 47\}$.

7 Results

We tested the the convolution based classical model (2) as well as maximum-slope model (3) for their capability to recover the perfusion values. The success of the restoration was measured voxelwise in terms of the relative error of the recovered perfusion with respect to the true perfusion

$$RE := \frac{|P_{\text{rec}} - P_{\text{true}}|}{P_{\text{true}}} \cdot 100\%.$$

Prior to reconstruction, the input data was downsampled to a time-resolution of 0.2 s. In order to simulate different spatial resolutions of the scanning process, the data was averaged using different block-sizes ranging from $(1, 1)$ to $(64, 64)$. Results are displayed in Figure 4 as well as in Table 2. Impuls response function reconstructed from the Porous Media Model are displayed in Figure 5.

Table 2: Results of the perfusion restoration with median relative errors in percent. Relative error was computed block-wise as $|P_{\text{rec}} - P_{\text{true}}|/P_{\text{true}} \cdot 100\%$. Displayed is the median RE over the entire domain. Abbreviations are: PMM - Porous Media Model, ConvM - Convolution Model.

	Model	Block Size			
		(1,1)	(5,5)	(10,10)	entire domain
PMM: Perfusion	MS	170.09	165.03	158.57	2.65
	bSVD	859.06	768.58	664.84	1.25
ConvM: Perfusion	MS	23.20	24.26	25.75	37.96
	bSVD	2.43	4.27	8.80	20.72
PMM: CBV		$4.37 \cdot 10^{-5}$	$4.37 \cdot 10^{-5}$	$4.37 \cdot 10^{-5}$	$4.37 \cdot 10^{-5}$
ConvM: CBV		$1.94 \cdot 10^{-2}$	$1.93 \cdot 10^{-2}$	$2.12 \cdot 10^{-2}$	1.13

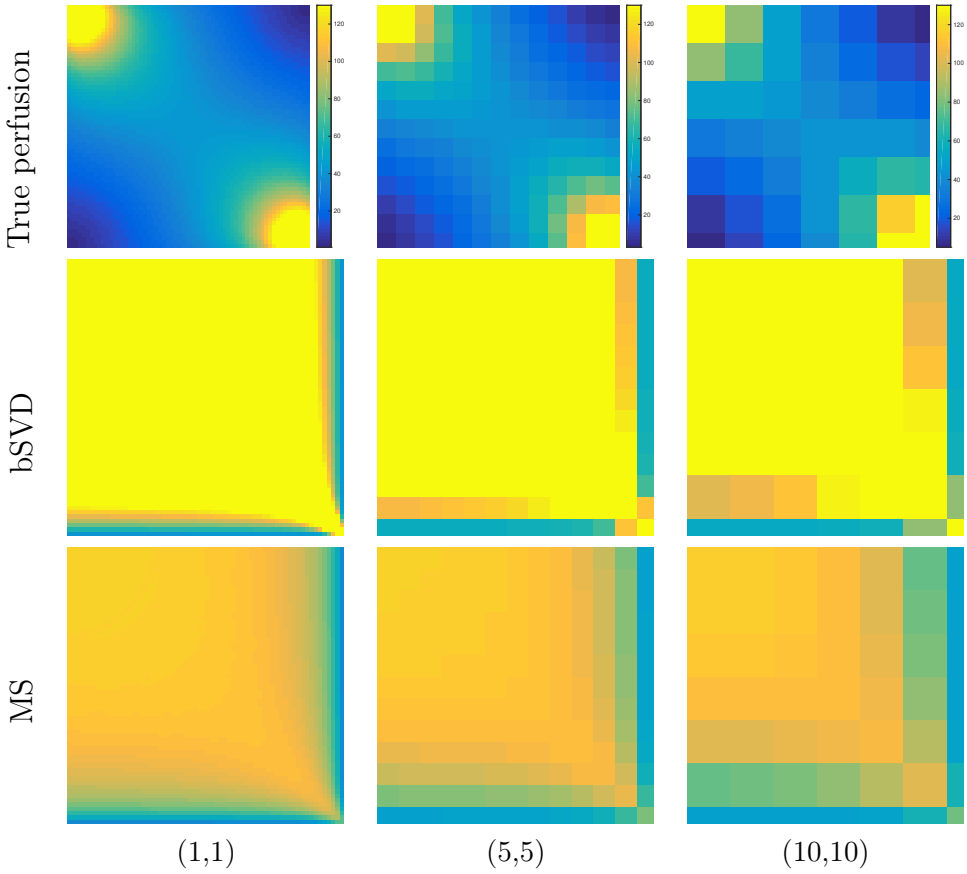

Figure 4: Results of the restoration of perfusion for the Porous Media Model (PMM) for different levels of discretization, displayed in the columns. All results are given in ml/min/100ml. First Row: Ground-Truth Perfusion (cf. Section 4.1). Second Row: Perfusion as estimated by bSVD. Third Row: Perfusion as estimated by the Maximum-Slope model.

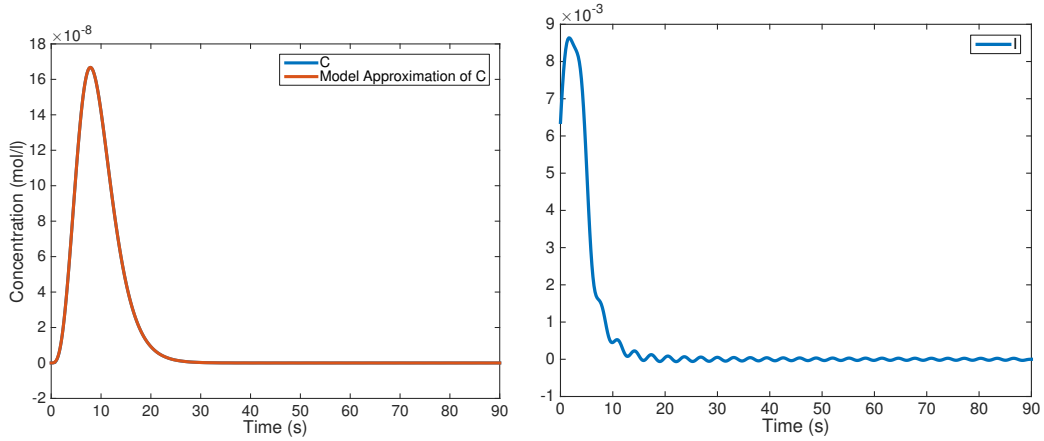

(a) Entire Domain, PMM

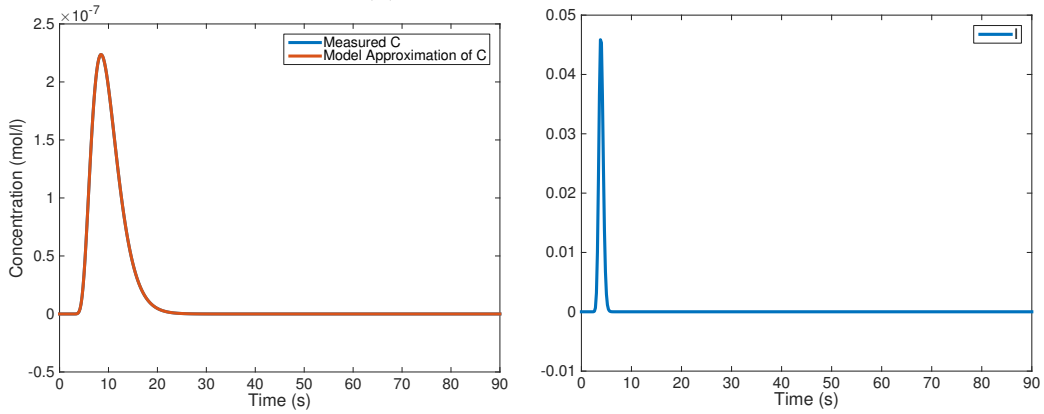

(b) Inside the capillary bed, PMM at $(i, j) = (50, 50)$

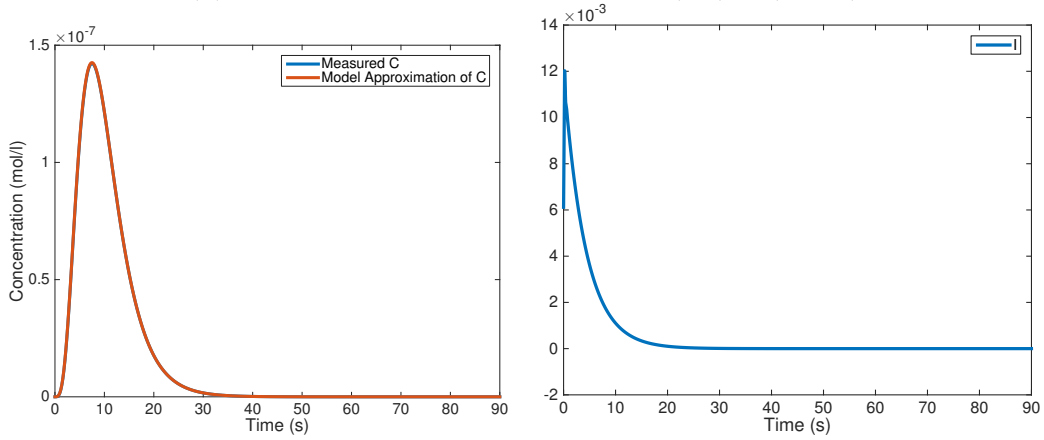

(c) Inside the capillary bed, ConvM at $(i, j) = (50, 50)$

Figure 5: Results for the deconvolution model. First row: Results of bSVD applied to PMM with block-size (64,64) (i.e. entire domain) (Model-Fit and Impuls-Response Function). Second row: Results of bSVD applied to a single voxel of the PMM in the inside of the domain. Third row: Second row: Results of bSVD applied to a single voxel of the SCD in the inside of the domain. In all cases the model restored the measured concentration curves perfectly.

8 Discussion

Results in Tab. 2 are indicating good performance of both models to restore the perfusion for an entire volume. Errors are 2.6% for the Maximum-Slope model and 1.3% for the deconvolution model. However, the results of the deconvolution model depend on a heuristic choice of the regularization parameter [?]. Results on a voxel-level are looking quite different (see Tab. 2). Here the perfusion is grossly overestimated by both the deconvolution model and the the maximum-slope model. Errors are in the range of far over 100%, indicating a lack of validity of the classic models. This impression is supported by the recovered impuls-response functions, displayed in Fig. 5. Although classic models assume monotonously decreasing residue-functions, the impuls-response functions we obtained are clearly violating this property. These effects might be due to dispersion effects [8] and are subject to current investigations.

However, as expected the deconvolution model worked quite good for the ConvM-dataset (see Tab. 2). But results are deteriorating if several volumes are averaged, leading to errors of up to 20%. This can be interpreted that even if the assumptions of the classical models are fulfilled, parameter-estimation will be sensitive with respect to broad resolutions. As already described in Sec. 6, the maximum-slope model fails to restore perfusion correctly due to the assumption of well-mixed compartments. Taking into account all of these observations we arrive at the following conclusions: If classical models are valid, a too broad spatial resolution might lead to significant errors in the estimation of perfusion parameters. On the other hand, a too fine resolution might lead to voxels placed inside of the capillary bed and hence to a dramatic overestimation of CBF. A method to determine the appropriate size of voxels is unknown to the authors, as it is coupled to the validity of the assumptions on the models.

Concluding, we have proposed a novel method to validate classical models for perfusion analysis. Based on porous media modeling, we described an easily extendable model to simulate CA-flow through a volume of interest. The proposed model assumes stationary and linearity of flow as well as spatially constant blood-volume. In this form it is completely in line with current pharmacokinetic modeling [7]. In order to connect (medical) volume perfusion with (physical) surface flow, a novel relationship between these two was introduced. For the experiments we have confined to a most simple setup, modeling a volume of interest with one inlet, one outlet and constant porosity. However, a more sophisticated simulation including more inlets and outlets at spatially varying locations as well as porosity can be set up readily. We showed that under these assumptions classical models are yielding good results for perfusion values and can indeed be used with high reliability. But as soon as the assumptions are violated, which is the case for the capillary bed, significant errors are introduced.

Since current validation of deconvolution algorithms is typically performed in the inverse-crime setting, the developed model could be used as an additional reference standard for validation. In the proposed modeling, exact perfusion values for the whole tissue can be

modeled. Using this method it is hence possible to quantify errors introduced by e.g. different numbers of input and output, more complex flow or even leakage.

As future work we will further investigate the impuls-response functions of the capillary bed and will simulate more complex phenomena in the tissue.

References

[1] K. L. Zierler, "Theoretical basis of indicator-dilution methods for measuring flow and volume," *Circ Res*, vol. 10, no. 3, pp. 393–407, 1962.

[2] L. Axel, "Cerebral blood flow determination by rapid-sequence computed tomography: theoretical analysis.," *Radiology*, vol. 137, no. 3, pp. 679–686, 1980.

[3] K. Zierler, "Indicator dilution methods for measuring blood flow, volume, and other properties of biological systems: a brief history and memoir," *Ann Biomed Eng*, vol. 28, no. 8, pp. 836–848, 2000.

[4] K. Kudo, M. Sasaki, K. Yamada, S. Momoshima, H. Utsunomiya, H. Shirato, and K. Ogasawara, "Differences in CT perfusion maps generated by different commercial software: Quantitative analysis by using identical source data of acute stroke patients 1," *Radiology*, vol. 254, no. 1, pp. 200–209, 2010.

[5] F. Calamante, D. L. Thomas, G. S. Pell, J. Wiersma, and R. Turner, "Measuring cerebral blood flow using magnetic resonance imaging techniques," *J Cerebr Blood F Met*, vol. 19, no. 7, pp. 701–735, 1999.

[6] N. Thacker, M. Scott, and A. Jackson, "Can dynamic susceptibility contrast magnetic resonance imaging perfusion data be analyzed using a model based on directional flow?," *J Magn Reson Im*, vol. 17, no. 2, pp. 241–255, 2003.

[7] S. Sourbron, "A tracer-kinetic field theory for medical imaging," *IEEE Trans Med Imaging*, 2014.

[8] F. Calamante, P. J. Yim, and J. R. Cebral, "Estimation of bolus dispersion effects in perfusion MRI using image-based computational fluid dynamics," *Neuroimage*, vol. 19, no. 2, pp. 341–353, 2003.

[9] L. Østergaard, R. M. Weisskoff, D. A. Chesler, C. Gyldensted, and B. R. Rosen, "High resolution measurement of cerebral blood flow using intravascular tracer bolus passages. part i: Mathematical approach and statistical analysis," *Magn Reson Med*, vol. 36, no. 5, pp. 715–725, 1996.

[10] B. Abels, E. Klotz, B. Tomandl, S. Kloska, and M. Lell, "Perfusion CT in acute ischemic stroke: a qualitative and quantitative comparison of deconvolution and maximum slope approach," *Am J Neuroradiol*, vol. 31, no. 9, pp. 1690–1698, 2010.

[11] M. Straka, G. W. Albers, and R. Bammer, "Real-time diffusion-perfusion mismatch analysis in acute stroke," *J Magn Reson Imaging*, vol. 32, no. 5, pp. 1024–1037, 2010.

[12] A. Bivard, C. Levi, N. Spratt, and M. Parsons, "Perfusion CT in acute stroke: a comprehensive analysis of infarct and penumbra," *Radiology*, vol. 267, no. 2, pp. 543–550, 2013.

[13] S. P. Sourbron and D. L. Buckley, "Classic models for dynamic contrast-enhanced MRI," *NMR in Biomedicine*, vol. 26, no. 8, pp. 1004–1027, 2013.

[14] K. Miles, "Measurement of tissue perfusion by dynamic computed tomography," *Br J Radiol*, vol. 64, no. 761, pp. 409–412, 1991.

[15] E. Klotz and M. König, "Perfusion measurements of the brain: using dynamic CT for the quantitative assessment of cerebral ischemia in acute stroke," *Eur J Radiol*, vol. 30, no. 3, pp. 170–184, 1999.

[16] R. Wirestam, L. Andersson, L. Østergaard, M. Bolling, J.-P. Aunola, A. Lindgren, B. Geijer, S. Holtås, and F. Ståhlberg, "Assessment of regional cerebral blood flow by dynamic susceptibility contrast MRI using different deconvolution techniques," *Magn Reson Med*, vol. 43, no. 5, pp. 691–700, 2000.

[17] T. Boutelier, K. Kudo, F. Pautot, and M. Sasaki, "Bayesian hemodynamic parameter estimation by bolus tracking perfusion weighted imaging," *IEEE T Med Imaging*, vol. 31, no. 7, pp. 1381–1395, 2012.

[18] K. Mouridsen, K. Friston, N. Hjort, L. Gyldensted, L. Østergaard, and S. Kiebel, "Bayesian estimation of cerebral perfusion using a physiological model of microvasculature," *Neuroimage*, vol. 33, no. 2, pp. 570–579, 2006.

[19] M. Sasaki, K. Kudo, T. Boutelier, F. Pautot, S. Christensen, I. Uwano, J. Goodwin, S. Higuchi, K. Ito, and F. Yamashita, "Assessment of the accuracy of a bayesian estimation algorithm for perfusion CT by using a digital phantom," *Neuroradiology*, vol. 55, no. 10, pp. 1197–1203, 2013.

[20] O. Wu, L. Østergaard, R. M. Weisskoff, T. Benner, B. R. Rosen, and A. G. Sorensen, "Tracer arrival timing-insensitive technique for estimating flow in mr perfusion-weighted imaging using singular value decomposition with a block-circulant deconvolution matrix," *Magn Reson Med*, vol. 50, no. 1, pp. 164–174, 2003.

[21] L. Evans, *Partial differential equations*. Providence, Rhode Island: American Mathematical Society, 2nd ed., 1998.

[22] A. A. Chan and S. J. Nelson, "Simplified gamma-variate fitting of perfusion curves," in *ISBI*, pp. 1067–1070, IEEE, 2004.

[23] R. Rosencranz and S. A. Bogen, "Clinical laboratory measurement of serum, plasma, and blood viscosity," *Am J Clin Pathol*, vol. 125 Suppl, pp. 78–86, Jun 2006.

[24] T. Kenner, "The measurement of blood density and its meaning," *Basic Res Cardiol*, vol. 84, no. 2, pp. 111–124, 1989.